

# Enabling Efficient Optimal Control of Reconfigurable Battery Systems by Unifying System Modeling and Narrowing Search Space

Changyou Geng, Dezhi Ren, Xinyi Zheng, Weiji Han, *Member, IEEE*

**Abstract**—Reconfigurable battery systems (RBSs) are emerging as a promising solution to improving fault tolerance, charge and thermal balance, energy delivery, etc. To optimize these performance metrics, high-dimensional nonlinear integer programming problems need to be formulated and solved. During this process, it is necessary to address multiple challenges stemming from nonlinear battery characteristics, discrete switch states, dynamic system configurations, as well as the curse of dimensionality inherent in large-scale systems. Thus, we propose a unified modeling framework to accommodate various potential configurations of an RBS and even to cover different RBS designs, significantly facilitating the topology design and optimization problem formulation for RBSs. Moreover, to solve the formulated RBS problems, the search space is tailored to encompass only feasible SSVs, thereby ensuring safe system operation while substantially curtailing search efforts. These proposed methods, focusing on unifying the system modeling and narrowing the search space, lay a solid foundation for effectively formulating and efficiently solving RBS optimal control problems. The accuracy and effectiveness of the proposed methods are demonstrated by simulation and experimental tests.

**Index Terms**—Reconfigurable battery systems, optimal control, battery system modeling, feasible solution space construction.

## I. INTRODUCTION

In response to the urgent imperative of mitigating greenhouse gas emissions, there has been a notable surge in the adoption of renewable energy sources by, e.g., solar panels and wind turbines [1]. Batteries, serving as a primary energy storage medium, play a pivotal role in both integrating renewable energy into power grids and facilitating its application to transportation electrification [2]. Given the intrinsic electrochemical nature of batteries, multiple batteries need to be connected either in series or in parallel to meet diverse voltage, current, or power demands across various applications. For multi-battery systems, inconsistent battery parameters and unbalanced operating states, such as state of charge (SoC), temperature, and state of health (SoH), result in a range of issues spanning from diminished energy delivery [3], accelerated degradation [4] to potential safety hazards [5]. Addressing these issues arising from unbalanced battery operation involves manipulating the operating currents of relevant batteries. However, in many practical battery systems, implementing individual current control becomes infeasible due to the commonly fixed battery connection configuration.

Aimed at mitigating the limitations imposed by fixed battery connections on system performance control, reconfigurable battery systems (RBSs), employing switches to dynamically

reconstruct battery connections, are emerging as a promising solution [6]. Various RBS designs, featuring diverse switch arrays and demonstrating different levels of reconfigurability, have been proposed [7]–[12]. For instance, Fig. 1 illustrates some RBS structure designs with two to five switches associated with each battery cell. Through switch operations, the battery connection can be reconfigured, enabling the recombination of battery terminal voltages and redistribution of currents among batteries. Then, by designing and implementing appropriate control algorithms, we can potentially improve the RBS’s operation performance in terms of enhanced fault tolerance [13], extended energy delivery [14], balanced battery states [15] and thermal distribution [16], and lower power efficiency [17]. Moreover, RBSs can accommodate batteries of different age, type and even chemistry [18], and facilitate the diagnosis, repair, and replacement of local batteries as well.

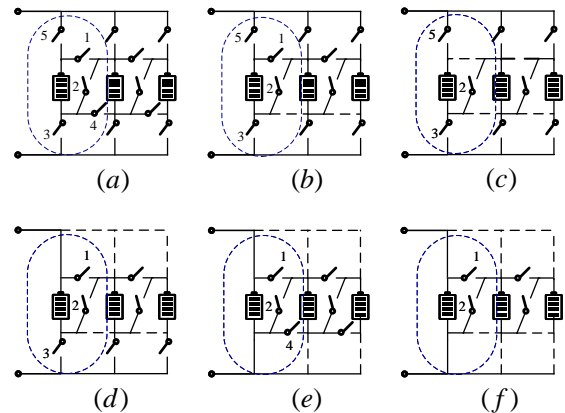


Fig. 1. Some structure designs for RBSs proposed in recent literature.

In order to fully leverage these potential benefits of RBSs, we need to formulate one specific optimal control problem, typically consisting of an objective function, a system plant, and some necessary constraints, as will be detailed in Section II. The system plant describing the system state evolution is formulated based on the electrical interconnection of all batteries, i.e., the system configuration. Thus, the system configuration, which can be specified by a switch state vector (SSV) describing the on-off states of all switches involved in the RBS, directly influences the evolution of system states and the value of objective function. Motivated by this, the system configuration is selected as one control variable. Through ap-

appropriate system reconfiguration, various system performance metrics defined in the objective function can get optimized.

When formulating and solving an RBS optimal control problem, a critical challenge is how to construct a system plant to model an RBS's dynamically varying system configuration, which has been rarely investigated in the literature. As the control variable, the RBS's configuration could vary within a wide range. The optimal system configuration is typically approached through an iterative evaluation-and-update process. During each iteration, a batch of configurations (or configuration series if multiple time steps are involved) are first evaluated and then updated according to certain principles. To evaluate the performance of a specific configuration, we need to construct its corresponding system plant, also called the system model, based on all battery cells' mathematical models as well as equations characterizing their electric connection according to Kirchhoff's current law (KCL) or voltage law (KVL) [19]. When evaluating another system configuration of the RBS, in which some battery units quit or join the operation and certain local series or parallel connections might change as well, it becomes difficult to directly revise the original system plant since some entry values and even the dimensions of system matrices might change. In this case, it is commonly necessary to construct a new system plant for the different system configuration. However, it is difficult to generate new plants automatically by programming codes due to involving re-indexing the batteries put into operation, rewriting their KCL and KVL equations, and reformulating the system matrices accordingly. Consequently, evaluating various system configurations by manually constructing different plants becomes very inefficient.

To address the issues caused by dynamic reconfiguration, a unified RBS modeling framework is proposed in this work. The formulated system plant, explicitly expressed in terms of the system configuration or SSVs, is capable of covering all possible configurations of an RBS without reconstruction, significantly reducing the computational efforts of evaluating various system configurations. In addition, thanks to the unified explicit expressions of the system plant, constraints for the system state transition can be formulated, allowing various commercial programming solvers to be applied directly.

When solving an RBS optimal control problem, another critical challenge is how to efficiently search the optimal solution. During the process of iterative evaluation and update, the number of possible system configurations experiences exponential growth with the number of switches involved in the RBS as well as the number of time steps within the control horizon, as will be demonstrated in Section IV. Thus, for large-scale RBSs, it becomes very time-consuming to search the optimal solution among a huge number of possible system configurations.

To alleviate the influence of the "curse of dimensionality", we propose to actively construct the feasible solution space. By filtering all SSVs incurring open circuits, short circuits, undesired system terminal voltage, or duplicate configurations, the size of the constructed feasible solution space is much smaller than that of the complete solution space exponentially expanding with the number of switches. In addition to ensuring

safe operation, the proposed method for narrowing the search space can dramatically enhance the search efficiency when optimizing certain RBS operating performance.

The reminder of this work are organized as follows. First, the general optimal control problem for RBSs will be formulated in Section II. In Section III, the unified modeling framework for RBSs will be introduced along with simulation and experimental tests to demonstrate the modeling accuracy. Then, the methodology to narrow the search space will be investigated in Section IV, and its performance will be compared with conventional methods. Finally, conclusions will be presented in Section V.

## II. OPTIMAL CONTROL PROBLEM FORMULATION FOR RBSS

A general optimal control problem is formulated as follows.

$$\begin{aligned} & \min J(X_0, U) \\ & \text{s.t.} \\ & X_k = \Phi(u_k, X_{k-1}), k = 1, 2, \dots, K, \\ & g_l(X_0, U) \geq 0, l = 1, 2, \dots, L, \\ & h_r(X_0, U) = 0, r = 1, 2, \dots, R, \\ & U \in \mathcal{U}^K. \end{aligned}$$

In the objective function  $J$ ,  $X_k$  denotes the system state at  $t = k\Delta t$ , and  $U = [u_1, u_2, \dots, u_K]$  the input trajectory, in which  $\Delta t$  is the duration of each time step, and  $K$  is the number of time steps considered during the optimization process. Among the constraints, the first one describes the system plant, followed by some inequality and equality constraints, and  $\mathcal{U}^K$  denotes the constraint set for the input trajectory.

Different from traditional battery systems, RBS enables the possibility to select the system configuration described by switch state vectors (SSVs) as one control variable or system input for the optimal control. Specifically, for the  $k$ -th time step  $((k-1)\Delta t, k\Delta t]$ , the corresponding input  $u_k$  is expressed as follows based on the on-off state of each switch, denoted by  $s_n \in \mathcal{B} = \{0, 1\}$ ,  $n = 1, 2, \dots, N_S$ , where  $N_S$  is the total number of switches in the RBS.

$$u_k = [s_1, s_2, \dots, s_{N_S}] \in \mathcal{B}^{N_S}. \quad (1)$$

The general process of iterative evaluation and update of SSVs for searching the optimal solution is illustrated in Fig. 2, in which the right part describes the performance evaluation of SSVs, the left part presents the search space of SSVs, and the optimization algorithms at the bottom generates the updated SSVs for each iteration. Among these three parts, the first two parts lay the foundation for adopting various optimization algorithms. Thus, this work will be mainly focused on boost the efficiency of evaluating and searching SSVs.

For efficiently evaluating the RBS performance metric described by the objective function  $J_k$ , in Section III we will develop a unified system plant with the SSV as input to accommodate diverse system configurations, corresponding to the unified state transition function  $\Phi(SSV, X)$  shown in Fig. 2. To further improve the searching efficiency, as shown in Fig. 2, instead of directly searching within the complete search

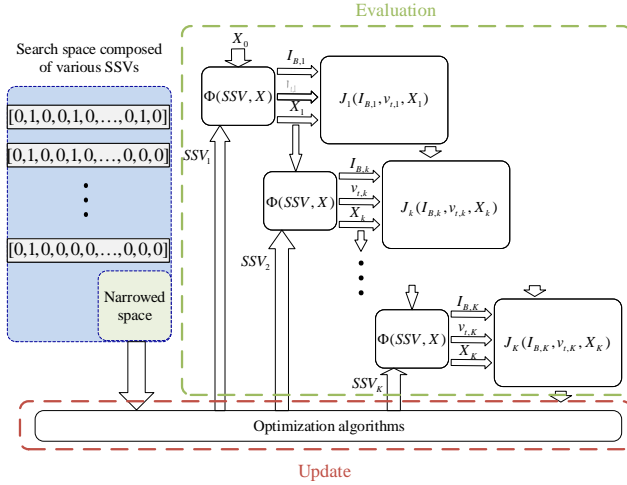


Fig. 2. Structural diagram of proposed framework.

space  $\mathcal{B}^{N_s}$ , we will identify only those feasible SSVs to form a dramatically narrowed search space in Section IV.

### III. UNIFIED MODELING FRAMEWORK FOR RBSS

Different structures can be designed for RBSs by changing the number of switches around each battery cell and the cell-switch connection pattern. For instance, as shown in Fig. 1, the RBS design (a) can encompass other designs (b)–(f) by selectively removing specific switch or wire branches (i.e., disconnecting the corresponding switches). Thus, we will take RBS design (a) as an example to introduce the unified modeling framework for RBSs.

#### A. Describing battery reconfiguration by switch resistance variables

To model an RBS, not only all components, including batteries, switches, wires, contactors, etc., but also the system configuration, i.e., how all components are interconnected with each other, needs to be described. The diagram for design (a) is presented in Fig. 3, in which the  $n$ -th battery cell,  $n = 1, 2, \dots, N_B$ , is represented by a second-order equivalent circuit model (ECM) [20], and  $N_B$  is the total number of battery cells. In this battery cell model,  $v_n$  denotes the open circuit voltage (OCV),  $R_{0,n}$  denotes the internal resistance, and two parallel resistor-capacitor (RC) pairs are used for describing the influence of the lithium diffusion process on the cell terminal voltage. Other types of battery models can be deployed as well if necessary. Around the  $n$ -th battery cell, the five switches are labeled as  $S_n^m$ ,  $m = 1, 2, \dots, 5$ , and each switch's state is denoted by  $s_n^m \in \{0, 1\}$ . If a switch's state is on, i.e., conductive,  $s_n^m = 1$  and its resistance is represented by its static drain to source on resistance  $R_{ds(on),n}^m$ . Otherwise,  $s_n^m = 0$  and the branch with an off-state switch can be removed.

Thus, the system configuration is not fixed but depends on the on or off switch states. When the RBS is dynamically reconfigured by switch operation, i.e., adjusting the states of certain switches, some local meshes in the diagram change

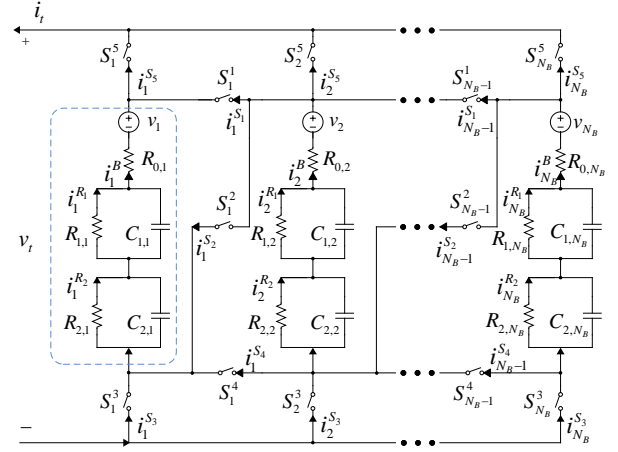


Fig. 3. Diagram for RBS design (a) in Fig. 1.

accordingly, as shown in Fig. 3. Consequently, we have to reconstruct the system model since some battery cells need to be re-indexed, and their corresponding KCL or KVL equations need to be rewritten as well.

To boost the modeling efficiency of RBSs by avoiding frequent system model reconstruction, it is desired to keep all meshes unchanged despite the dynamic battery reconfiguration. Thus, instead of directly removing those off-state switch branches, all branches are reserved to form the same meshes during reconfiguration. Further, to reflect the changes in switch states, different resistances are assigned to switches with on and off states, and they are combined into a switch resistance variable  $R_n^{S_m}$  through the binary switch state  $s_n^m$ , as proposed in (2). In this expression,  $R_{ds(off),n}^m$  denotes the switch's drain to source off resistance, which is typically at  $M\Omega$  level for practical MOSFETs [21]. Moreover, to simplify the denotation, the resistance of the connection wire along the switch branch, denoted by  $R_{wire,n}^m$ , is incorporated into  $R_n^{S_m}$ .

$$R_n^{S_m} = s_n^m R_{ds(on),n}^m + (1 - s_n^m) R_{ds(off),n}^m + R_{wire,n}^m. \quad (2)$$

According to (2), the switch branch's resistance  $R_n^{S_m} = R_{ds(on),n}^m + R_{wire,n}^m$  if the switch is on, or  $R_n^{S_m} = R_{ds(off),n}^m + R_{wire,n}^m$  if the switch is off. Then, any switch state change corresponding to the dynamic reconfiguration can be reflected by the finite value of the switch resistance variable. Through this way, those off-state switch branches are reserved, and we can always maintain a *full system configuration* (FSC) involving all switch, battery, and wire branches. Once an SSV is specified by all switch states, all switch resistances will be determined based on (2), and the corresponding system configuration FSC(SSV) will be obtained. Most importantly, the FSC features stable meshes regardless of the reconfiguration, significantly facilitating the formulation of KCL and KVL equations. Thanks to this property of the FSC, it becomes possible to develop a unified system plant to cover all system configurations of an RBS.

### B. Formulation of the unified RBS model

To formulate the state-space representation for the RBS plant or model based on the system's FSC, the states of battery cells shown in Fig. 3, including each cell's the resistor currents  $i_{n_1}^{R_1}$  and  $i_{n_2}^{R_2}$  in the RC pairs and the OCV  $v_n$ , are chosen to compose the RBS's state vector as follows.

$$X = [V^T, I_{R_1}^T, I_{R_2}^T]^T. \quad (3)$$

In the above state vector,  $V = [v_1, v_2, \dots, v_N]^T$  is the vector of battery cell OCVs, and  $I_* = [i_1^*, i_2^*, \dots, i_N^*]^T$  denotes the current vector of all components specified by the wildcard  $*$ . For instance,  $I_B$ ,  $I_{S_m}$ , and  $I_{R_1}$  represent the current vectors of all battery cells, all the  $m$ -th switches around battery cells, all  $R_1$  in the battery cell ECMs, respectively. In addition, the system's total current  $i_t$  is regarded as one input. The system's output can be selected according to the objective function  $J$ .

For each battery cell, the current  $i_n^B = dQ_n/dt$ ,  $n = 1, 2, \dots, N_B$ , where  $Q_n$  denotes the cell's amount of charge. Each cell's SoC  $z_n = Q_n/Q_{C,n}$ , where  $Q_{C,n}$  denotes its charge capacity. The slope of the cell's OCV-SoC curve at  $z_n$  is defined by  $k_n^V(z) = dv_n/dz_n$ . Then, the evaluation of each cell's OCV is described by

$$\dot{v}_n = \frac{dv_n}{dt} = \frac{dv_n}{dz_n} \frac{dz_n}{dt} = \frac{k_n^V(z)}{Q_{C,n}} \frac{dQ_n}{dt} = \frac{k_n^V(z)}{Q_{C,n}} i_n^B, \quad (4)$$

and the corresponding matrix form for the OCV vector is

$$\dot{V} = B_V I_B. \quad (5)$$

To derive the state-space equations describing the evolution of  $I_{R_1}$  and  $I_{R_2}$  in the state vector  $X$ , KCL and KVL equations need to be formulated based on the FSC in Fig. 3, where  $i_n^{S_m}$  denotes the current of the  $m$ -th switch around the  $n$ -th cell,  $m = 1, 2, \dots, 5$ ,  $n = 1, 2, \dots, N_B$ . The KCL equations at the positive and negative electrodes of the  $n$ -th cell are formulated as follows.

$$\begin{cases} -i_n^B - i_n^{S_1} + i_n^{S_5} = 0, & \text{if } n = 1, \\ -i_n^B - i_n^{S_1} + i_n^{S_5} + i_{n-1}^{S_1} + i_{n-1}^{S_2} = 0, & \text{if } 1 < n < N_B, \\ -i_n^B + i_n^{S_5} + i_{n-1}^{S_1} + i_{n-1}^{S_2} = 0, & \text{if } n = N_B. \end{cases} \quad (6)$$

$$\begin{cases} i_n^B - i_n^{S_2} - i_n^{S_3} - i_n^{S_4} = 0, & \text{if } n = 1, \\ i_n^B - i_n^{S_2} - i_n^{S_3} - i_n^{S_4} + i_{n-1}^{S_4} = 0, & \text{if } 1 < n < N_B, \\ i_n^B - i_n^{S_3} + i_{n-1}^{S_4} = 0, & \text{if } n = N_B. \end{cases} \quad (7)$$

At the positive and negative terminals of the RBS, the KCL equations are formulated as follows.

$$\sum_{n=1}^N i_n^{S_5} = i_t, \quad (8)$$

$$\sum_{n=1}^N i_n^{S_3} = i_t. \quad (9)$$

For the four meshes between the  $n$ -th and  $(n+1)$ -th cells,  $1 \leq n < N_B$ , the KVL equations are formulated as follows.

$$R_n^{S_5} i_n^{S_5} - R_{n+1}^{S_5} i_{n+1}^{S_5} + R_n^{S_1} i_n^{S_1} = 0, \quad (10)$$

$$R_{0,n} i_n^B - v_n - R_n^{S_1} i_n^{S_1} + R_n^{S_2} i_n^{S_2} + R_{1,n} i_n^{R_1} + R_{2,n} i_n^{R_2} = 0, \quad (11)$$

$$R_{0,n+1} i_{n+1}^B - v_{n+1} + R_{1,n+1} i_{n+1}^{R_1} + R_{2,n+1} i_{n+1}^{R_2} + R_n^{S_2} i_n^{S_2} - R_n^{S_4} i_n^{S_4} = 0, \quad (12)$$

$$R_n^{S_3} i_n^{S_3} - R_{n+1}^{S_3} i_{n+1}^{S_3} - R_n^{S_4} i_n^{S_4} = 0. \quad (13)$$

In the above KCL and KVL equations, it is aimed to cancel all intermediate variables,  $i_n^B$ ,  $i_n^{S_m}$ ,  $n = 1, 2, \dots, N_B$ ,  $m = 1, 2, \dots, 5$ , so that only state variables in  $X$  and the system input  $i_t$  are left in the final state-space equations. At first, intermediate variables  $i_n^{S_1}$  and  $i_n^{S_4}$ ,  $1 \leq n < N_B$ , can be expressed as (14) and (15) based on (6) and (7), respectively.

$$i_n^{S_1} = -i_n^B + i_n^{S_5} + \sum_{j=2}^n (-i_j^B + i_j^{S_5} + i_{j-1}^{S_2}), \quad (14)$$

$$i_n^{S_4} = \sum_{j=1}^n (i_j^B - i_j^{S_2} - i_j^{S_3}). \quad (15)$$

After substituting all  $i_n^{S_1}$  and  $i_n^{S_4}$  in (10)-(13) using (14) and (15), KVL equations (10)-(13) are combined with KCL equations (8) and (9) and then reorganized into the following matrix forms to facilitate the derivation, where  $E_*$ ,  $F_*$ ,  $G_*$ , and  $H_*$  are  $N_B \times N_B$  coefficient matrices of the corresponding current vectors. To have square matrices  $F_{S_2}$  and  $G_{S_2}$ , a virtual switch current  $i_{N_B}^{S_2} = 0$  is appended to form a  $N_B \times 1$  vertical vector  $I_{S_2}$ .

$$E_{S_5} I_{S_5} = E_B I_B + E_{S_2} I_{S_2} + E_t i_t, \quad (16)$$

$$F_{S_2} I_{S_2} = F_B I_B + F_{R_1} I_{R_1} + F_{R_2} I_{R_2} + F_v V + F_{S_5} I_{S_5}, \quad (17)$$

$$G_{S_2} I_{S_2} = G_B I_B + G_{R_1} I_{R_1} + G_{R_2} I_{R_2} + G_v V + G_{S_3} I_{S_3}, \quad (18)$$

$$H_{S_3} I_{S_3} = H_B I_B + H_{S_2} I_{S_2} + H_t i_t. \quad (19)$$

By substituting the  $I_{S_5}$  in (17) with the  $I_{S_5}$  derived from (16), we can obtain (20). Similarly, the  $I_{S_3}$  in (18) can be substituted with the one obtained from (19), leading to (21).

$$J_{S_2} I_{S_2} = J_B I_B + J_{R_1} I_{R_1} + J_{R_2} I_{R_2} + J_v V + M_t i_t, \quad (20)$$

$$K_{S_2} I_{S_2} = K_B I_B + K_{R_1} I_{R_1} + K_{R_2} I_{R_2} + K_v V + K_t i_t. \quad (21)$$

Through combining (20) and (21),  $I_{S_2}$  can be eliminated. Then, the cell current vector  $I_B$  can be expressed as follows based on the state vector defined in (3).

$$I_B = C_{I_B} X + D_{I_B} i_t. \quad (22)$$

The derived equation (22) plays an important role in bridging the gap between the battery system-level current  $i_t$  and all cell-level currents in  $I_B$ . According to the battery cell ECMs in Fig. 3, we have

$$I_B = I_{R_1} + T_1 \dot{I}_{R_1} = I_{R_2} + T_2 \dot{I}_{R_2}, \quad (23)$$

where  $\dot{I}_* = dI_*/dt$ , and  $T_1$  and  $T_2$  represent  $N_B \times N_B$  diagonal matrices with the RC pairs' time constants  $\tau_{1,n} = R_{1,n}C_{1,n}$  and  $\tau_{2,n} = R_{2,n}C_{2,n}$  as the  $n$ -th diagonal entries, respectively. Then, combining (22) and (23) leads to the following state-space equations characterizing the evolution of  $I_{R_1}$  and  $I_{R_2}$ , respectively.

$$\dot{I}_{R_1} = A_{I_{R_1}} X + B_{I_{R_1}} i_t, \quad (24)$$

$$\dot{I}_{R_2} = A_{I_{R_2}} X + B_{I_{R_2}} i_t. \quad (25)$$

Finally, based on the defined state vector  $X$  in (3), we can reorganize all state evolution equations in (5), (24), and (25) to formulate the state-space model or plant for the battery system as follows.

$$\dot{X} = AX + Bi_t. \quad (26)$$

In order to pursue higher computational efficiency and match the discrete-time system plant in the formulated optimal control problem at the beginning of Section III, the state-space model in (26) can be further discretized according to, e.g., the Euler method. During each time step, battery ECM parameters might change with battery states and temperatures, and, thus, they need to be updated within the time step, leading to a time-varying system model.

Based on the system plant formulated in (26), we can derive the expression for any system output of interest, such as the cell current vector  $I_B$ , cell terminal voltage vector denoted by  $V_B$ , and the system's terminal voltage denoted by  $v_t$  as shown in Fig. 3.  $I_B$  is already expressed in (22) in terms of the system's state vector  $X$  and input  $i_t$ . Denote the terminal voltage of the  $n$ -th battery cell by  $v_n^B$ ,  $n = 1, 2, \dots, N_B$ . Then, the cell terminal voltage vector is  $V_B = [v_1^B, v_2^B, \dots, v_{N_B}^B]^T$ . According to the battery cell ECM in Fig. 3,

$$v_n^B = v_n - R_{0,n}i_n^B - R_{1,n}i_n^{R_1} - R_{2,n}i_n^{R_2}, \quad (27)$$

$$v_t = v_n^B - R_n^{S_3}i_n^{S_3} - R_n^{S_5}i_n^{S_5}. \quad (28)$$

Then,  $V_B$  can be expressed as follows based on (3), (22), and (27).

$$V_B = C_{V_B} X + D_{V_B} i_t. \quad (29)$$

Specify one battery cell  $n$  in (28), and then based on (16), (19), (20), (22), and (29), the battery system's terminal voltage can be expressed as follows

$$v_t = C_{v_t} X + D_{v_t} i_t. \quad (30)$$

Due to the instability of the terminal voltage in RBSs, the input current is influenced not only by the load power but also by the system configuration. Here, we present a simple and accurate method for determining the input current, with its accuracy demonstrated in Section III-C. Based on (30), given a power request  $p_t$  during each time step in practical applications of battery systems, the system's input current  $i_t$  can be calculated by solving the quadratic equation

$$p_t = v_t i_t = C_{v_t} X i_t + D_{v_t} i_t^2. \quad (31)$$

During the above formulation of a unified RBS state-space model, it is worth noting that, the specified SSV for each time step determines the switch resistances in the KVL equations (10)-(13) through the proposed switch resistance variable in

TABLE I  
12 FEASIBLE CONFIGURATIONS OF THE RBS DESCRIBED BY SSVs.

Config. index	SSV	Config. index	SSV
1	[1,0,0,0,0,1,0]	7	[1,0,0,1,0,1,1]
2	[1,0,0,1,0,0,1]	8	[1,0,1,1,0,1,1]
3	[1,0,0,0,1,0,1]	9	[0,1,0,0,1,0,1]
4	[0,1,0,1,0,0,1]	10	[0,1,0,0,0,1,0]
5	[0,1,0,1,0,1,1]	11	[1,0,1,0,0,0,0]
6	[1,0,1,1,0,0,1]	12	[1,0,1,0,0,1,0]

(2), and, hence, affects the system matrices in the system plant (26) and the output matrices in the output equations, such as (22), (29), and (30). This indicates that the evolution of system state variables and output variables can be controlled through adjusting the SSV. As previously mentioned, since the RBS design (a) encompasses other designs (b)–(f) shown in Fig. 1, their system plant can be constructed by selectively fixing the corresponding switch states in SSV to 0.

### C. Model validation by simulation and experimental tests

To evaluate the simulation accuracy of the proposed RBS modeling framework during the operation as well as dynamic reconfiguration, a three-cell RBS was designed based on the structure in Fig. 1 (d), consisting of three cells and seven switches indexed from 1 to 7. The RBS was discharged with a constant load power of 8 W. During the discharging process, the battery system was sequentially reconfigured every 20 seconds to each configuration described by the SSV in Table I.

To simulate the system operation and dynamic reconfiguration using the developed RBS model, we need to identify all parameter values of battery cells, switches, and wires. For each deployed EVE ICR 18650 battery cell, the ECM parameters were identified through Hybrid Pulse Power Characterization (HPPC) test data [22] based on trust-region-reflective method, resulting in mean absolute errors (MAEs) of 0.8 mV, 1.0 mV, and 1.1 mV for the three cells. For each switch, two N-channel MOSFETs are connected in series to enable bidirectional current blocking. When using (2) to calculate each switch's resistance,  $R_{ds(on),n}^m = 4 \text{ m}\Omega$  according to the datasheet,  $R_{wire,n}^m = 4 \text{ m}\Omega$  based on the measurement, and  $R_{ds(off),n}^m$  is approximately 2 M $\Omega$  estimated from the drain current and drain-source voltage at zero gate voltage and room temperature.

To conduct the discharge test of the RBS, a testbed was set up, as shown in Fig. 4. Particularly, a drive circuit was designed for the MOSFET switch, and they were integrated on a printed circuit board (PCB) according to the RBS structure design in Fig. 1 (d). The RBS was discharged with a constant power by a direct current (DC) load. A data acquisition module is used to collect the voltage and current measurement data of battery cells at a sampling frequency of 10 Hz. Based on the collected measurement data, a desktop computer and a National Instruments (NI) controller are deployed to generate control signals and send them to the drive circuit of switches.

In Fig. 5, when the battery system is sequentially reconfigured from Config. 1 to Config. 12 every 20 seconds, the

- 1 NI controller      2 DC load      3 Batteries      4 Switch array
- 5 DC-DC converter    6 Desktop monitor    7 Power supply

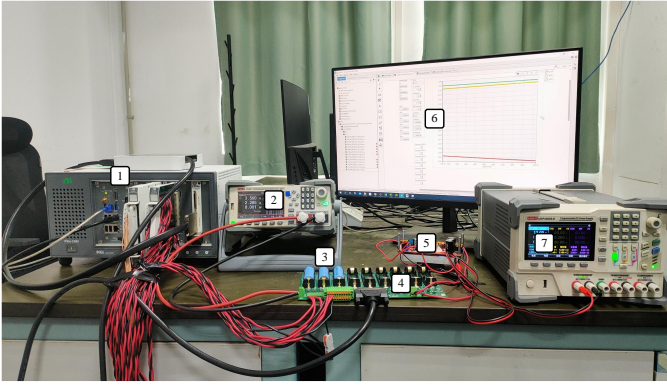


Fig. 4. Illustration of the testbed for RBS experiments.

simulated evolution of the system’s terminal voltage and input current, based on (30) and (31) in the proposed unified RBS model, are compared with experimental measurement. The simulation MAEs are 52 mV and 46 mA, respectively. Due to system reconfiguration, both terminal voltage and input current change accordingly despite the constant discharge power.

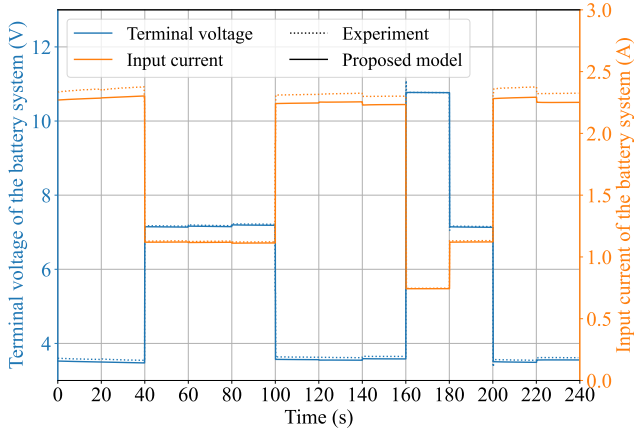


Fig. 5. Comparison of the battery system’s terminal voltage and input current obtained from model-based simulation with experimental measurement.

In addition to the system-level simulation, the simulated cell-level currents and voltages obtained from a simple model and the proposed model are compared with experimental results in Figures 6 and 7, respectively. The simple model shares the same battery parameter values with the proposed model, but the total current is always assumed to be equally divided among parallel branches by neglecting the resistances of switches and wires in the simple model. According to the simulation MAEs for the proposed and simple models compared in Table II, we can see that the cell-level simulation results from the proposed model have current MAEs  $\leq 20$  mA and voltage MAEs  $\leq 7$  mV, much lower than those from the commonly used simple model assuming even parallel current distribution. The low simulation MAEs of the proposed model are mainly attributed to its capability of accurately

characterizing the time-varying uneven current distribution among parallel cells during time intervals such as 80~160 seconds and 220~240 seconds in Fig. 6, corresponding to Config. 5 to Config. 8 and Config. 12 in Table I, respectively. In such configurations with parallel connections, it is of great importance to capture the dynamic current distribution for improving the state estimation accuracy and keeping the safe system operation.

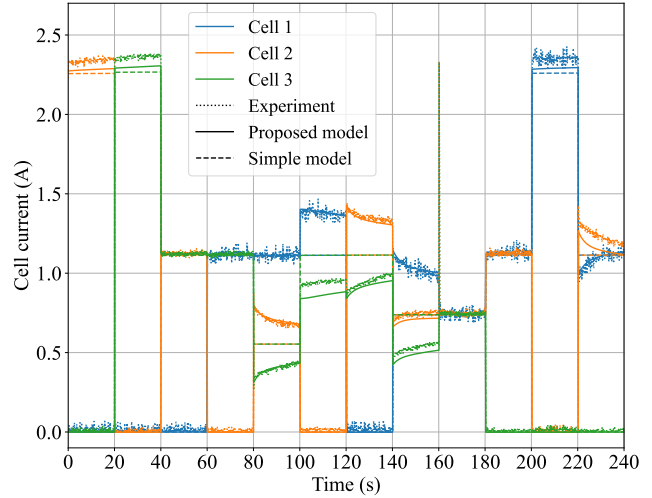


Fig. 6. Comparison of the cell current evolution obtained by model-based simulation with experimental results.

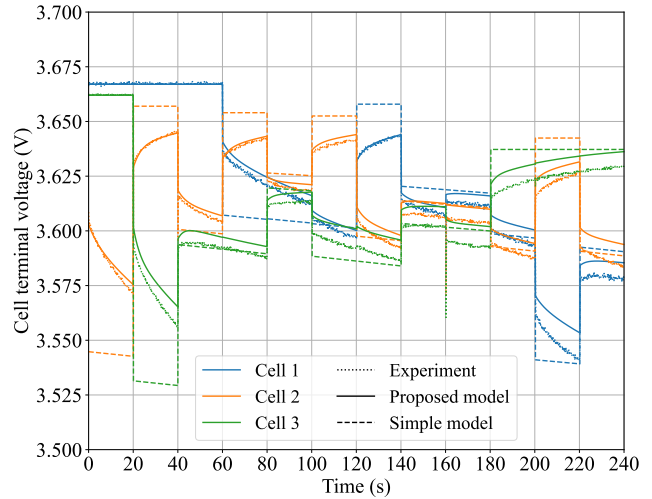


Fig. 7. Comparison of the cell terminal voltage evolution obtained by model-based simulation with experimental results.

In general, the simulated voltages and currents at system and cell levels based on the proposed unified RBS model can align well with the experimental measurement, except for some transient pulses. When reconfiguring the system from Config. 8 to Config. 9 at 160 s, some current or voltage pulses can be observed in Fig. 5, Fig. 6, and Fig. 7 due to suffering from a short circuit fault during the switch operations. Fortunately, by considering the delay of control signals and appropriately

TABLE II  
MAE OF PROPOSED AND SIMPLE MODEL.

Cell index	Proposed model			Simple model		
	1	2	3	1	2	3
Cell current (mA)	19	20	20	69	60	74
Terminal voltage of cell (mV)	3.8	5.1	6.7	7.7	11.7	8.8

designing the sequence of switch operations, the duration of such short circuit faults can be well restricted to minimize their impact on operation safety and performance control.

#### IV. CONSTRUCTION OF NARROWED SEARCH SPACE

After addressing the critical challenge of formulating a unified RBS plant in Section III, we are still confronted with the issue of low search efficiency when solving the formulated optimal control problems since the search space  $\mathcal{B}^{N_s}$  grows exponentially with the increasing number of switches  $N_s$ . In this section, we will develop a framework to narrow the search space for high efficiency as well as safe connections. At first, the mapping relation between a system configuration and a system SSV will be established. Then, an algorithm will be developed to enumerate all feasible system configurations. Finally, based on the established mapping relation, only those feasible system configurations will be converted to feasible SSVs to construct a feasible search space  $\mathcal{B}_f^{N_s}$ . By tailoring the search scope from all system configurations to only those feasible ones, the size of the constructed feasible search space is expected to be much smaller than that of the complete search space. Since the RBS design (a) in Fig. 1 can be turned into other designs (b)-(f) by always connecting certain switches, it is taken as an example for introduce how to narrow the search space.

##### A. Mapping a system configuration with a system SSV

In a battery system, all battery cells connected in series (or parallel) in a local area form an internally series-connected (or parallel-connected) battery module, referred to as a *series* (or *parallel*) *module*, denoted by  $M_s$  (or  $M_p$ ). If one single cell does not fall into any series or parallel module, it is regarded as a  $M_s$  (or  $M_p$ ) if cells are connected in series (or parallel) in its neighboring module. Similarly, all local battery modules can construct a *series* or *parallel battery pack*. Through analyzing the feasible configurations of the RBS design (a), we can see that some battery cells can be selected to form only series modules, and all series modules can then constitute a parallel pack. This is referred to as a *series-then-parallel configuration*, denoted by  $C_{sp}$ . On the other hand, battery cells can be selected to form some series and parallel modules, and all modules can then constitute a series pack. Such a configuration is referred to a *parallel-then-series configuration*, denoted by  $C_{ps}$ . However, at most one battery pack can be constructed among all feasible configurations of the RBS design (a).

In such a hierarchical description of a battery pack, each battery cell belongs to one unique associated module, and further one unique associated pack. Once a battery cell's position and connection pattern (e.g., series, parallel, or single)

within its associated module as well as its associate module's position and connection pattern (P&CP) within its associated pack are specified, the state vector of all associated switches with the cell, referred to as a *cell SSV*, will be determined. All cell SSVs compose the RBS's SSV, and, thus, describes the system's configuration. For instance, for the circled cell in the RBS design (a) in Fig. 1, its cell SSV consists of the states of switches 1 to 5. The P&CPs of a battery cell and its associated module are referred to as *cell-module P&CPs*.

All possible cell-module P&CPs are summarized in Table III, and the corresponding cell SSVs are listed and indexed. These cell SSVs are illustrated in Fig. 8 as well. As shown in Table III, different cell-module P&CPs can be described by the same cell SSV. Moreover, if multiple cell SSVs lead to the same cell-module P&CPs, only one of them is reserved in Table III. For instance, a cell can get connected to the next cell in parallel to construct a parallel module by connecting switches 4 and 5 (i.e., cell SSV (4)), switches 1 and 4 (i.e., cell SSV (5)), or switches 1 and 3 (i.e., cell SSV (6)). Among these three cell SSVs, the first and third ones can facilitate bypassing cells but they need the top or bottom bus lines for linking the two battery system terminals. Thus, cell SSVs (4) and (6) are deployed to construct the parallel modules at the beginning and end of a configuration, respectively.

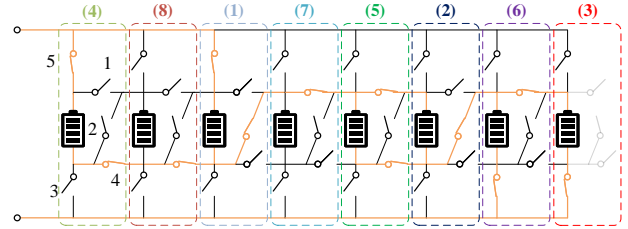


Fig. 8. Examples of all eight possible cell connection patterns in the RBS design (a) in Fig. 1.

Thus, given any configuration of a battery pack, we can identify each cell's cell-module P&CPs and look up its corresponding cell SSV based on Table III. All the obtained cell SSVs are then used to construct the system SSV. Next, in order to formulate the feasible search space of system SSVs we need to identify all those feasible system configurations.

##### B. Identifying all feasible system configurations

As introduced in Section I, the RBS features a wide range of terminal voltages, which can be divided into multiple levels. For an RBS with  $N_B$  cells, the system's *terminal voltage level*  $L_{v_t}$  is set to  $n_s \in \{1, \dots, N_B\}$  if we have  $n_s$  series-connected battery cells along the connection path between the system's positive and negative terminals. Among all configurations of an  $N_B$ -cell RBS, there exist a majority of infeasible system configurations resulting in short circuit faults, unacceptable terminal voltage levels, or undesired open circuits. An algorithm will be developed to identify the remaining feasible configurations, only having safe connections and meeting the required terminal voltage level  $L_{v_t}^{req} \in \{L_{v_t}^{min}, \dots, L_{v_t}^{max}\}$ .

TABLE III  
CELL SSVs FOR ALL POSSIBLE CELL-MODULE P&CPs IN THE RBS DESIGN (A) IN FIG. 1.

Cell-module P&CPs	Cell SSV	Index
The first cell in a $M_s$ in a $C_{sp}$ , a $M_s$ at the beginning of a $C_{ps}$ , or the last cell in a $M_p$ at the beginning of a $C_{ps}$ .	[0, 1, 0, 0, 1]	(1)
Middle cells in a $M_s$ in a $C_{sp}$ , cells in a $M_s$ in a $C_{ps}$ , or the last cell in a $M_p$ at the middle of a $C_{ps}$ .	[0, 1, 0, 0, 0]	(2)
The last cell in a $M_s$ at the end of a $C_{ps}$ , a $M_s$ in a $C_{sp}$ , or a $M_p$ at the end of a $C_{ps}$ .	[0, 0, 1, 0, 0]	(3)
The first cell or middle cells in a $M_p$ at the beginning of a $C_{ps}$ .	[0, 0, 0, 1, 1]	(4)
The first cell or middle cells in a $M_p$ at the middle of a $C_{ps}$ .	[1, 0, 0, 1, 0]	(5)
The first cell or middle cells in a $M_p$ at the end of a $C_{ps}$ .	[1, 0, 1, 0, 0]	(6)
The bypassed cell in a $M_s$ in a $C_{ps}$ , or a $M_p$ at the middle or end of a $C_{ps}$ .	[1, 0, 0, 0, 0]	(7)
The bypassed cell in a $M_p$ at the beginning of a $C_{ps}$ , or a $M_s$ in a $C_{sp}$ .	[0, 0, 0, 1, 0]	(8)

In a series-then-parallel configuration  $C_{sp}$ , all series-connected cells in each series module  $M_s$  along with those bypassed cells in between are neighboring cells, and all  $M_s$ 's need to meet the required system terminal voltage level  $L_{vt}^{req}$ , indicating that each  $M_s$  must have  $L_{vt}^{req}$  cells. Moreover, any cell in a  $C_{sp}$  can be bypassed. Denote all battery cells with indices from 1 to  $N_B$ , the  $j$ -th series module by  $M_{s,j}$ , and the total number of series modules by  $N_{M_s}$ . Then, a  $C_{sp}$  can be constructed as follows by sequentially selecting  $L_{vt}^{req}$  battery cells for each series module while skipping those bypassed cells. As a result, a total of  $\sum_{m=2}^{\lfloor \frac{N_B}{L_{vt}^{req}} \rfloor} \binom{mL_{vt}^{req}}{N_B}$  feasible  $C_{sp}$ 's are obtained, in which  $\binom{mL_{vt}^{req}}{N_B}$  calculates a binomial coefficient.

$$\begin{aligned}
 M_{s,j} &= (k_{j,1}, k_{j,2}, \dots, k_{j,L_{vt}^{req}}), \\
 1 &\leq k_{j,1} < k_{j,2} < \dots < k_{j,L_{vt}^{req}} < k_{j+1,1} \leq N_B, \\
 C_{sp} &= (M_{s,1}, M_{s,2}, \dots, M_{s,N_{M_s}}), \\
 N_{M_s}, j &\in \mathbb{Z}, 1 < N_{M_s} \leq \frac{N_B}{L_{vt}^{req}}, j \leq N_{M_s}.
 \end{aligned}$$

Different from the above series-then-parallel configurations allowing only series modules with the same number of cells and arbitrary cell bypassing, a parallel-then-series configuration  $C_{ps}$ 's allows both series and parallel modules, and the number of cells in each module can differ from each other. Moreover, in the  $C_{ps}$ 's of the RBS design (a), all cells can be bypassed except those in a  $M_p$  at the middle of a  $C_{ps}$ . Consequently, it becomes more difficult to identify all feasible  $C_{ps}$ 's. To address this challenge, Algorithm 1 is developed to identify all  $C_{ps}$ 's using dynamic programming. As shown in Algorithm 1, the cell-module P&CPs listed in Table III are further aggregated, and five types of position flags of battery cells are defined, including the cell bypassing. Then, a vector consisting of all cell position flags is used to describe a  $C_{ps}$ . To accommodate all cell flag vectors, a three-dimension list  $D$  is constructed. Next, dynamic programming (DP) is deployed to search for the cell flag vectors corresponding to all feasible  $C_{ps}$ . DP creates sets iteratively, leveraging information from previously established sets to optimize brute-force enumeration. By storing and reusing intermediate results, it avoids redundant calculations and significantly reduces time complexity.

Finally, according to the mapping relation established in Table III, all the identified feasible  $C_{sp}$ 's and  $C_{ps}$ 's are translated to feasible SSVs, which compose the feasible search space for system SSVs  $\mathcal{B}_f^{Ns}$ . Due to the fact that RBS design

(a) encompasses other designs (b)–(f) shown in Fig. 1, their feasible search space can be constructed by excluding the SSVs that assign a state of 1 to switches that are absent in the designs.

### C. Quantifying the narrowing effect of the proposed feasible search space

To demonstrate the narrowing effect of the identified feasible search space  $\mathcal{B}_f^{Ns}$  as compared with the complete search space  $\mathcal{B}^{Ns}$ , the numbers of feasible SSVs for various cell numbers and terminal voltage levels, denoted by  $N_f(N_B, L_{vt})$ 's, are summarized and compared with the number of all possible SSVs in Table IV. For an  $N_B$ -cell RBS, the total number of feasible SSVs across all terminal voltage levels is  $\sum_{L_{vt}=1}^{N_B} N_f(N_B, L_{vt})$ . For the same system size  $N_B$ , the total number of possible SSVs is  $2^{5N_B-3}$  since each cell is associated with 5 switches except that the last one has only 2 switches as shown in Fig. 1 (a). As can be seen in Table IV, both the total number of feasible SSVs in  $\mathcal{B}_f^{Ns}$  and the total number of possible SSVs in  $\mathcal{B}^{Ns}$  grows as the system size  $N_B$  increases, but the former is much smaller than the latter and their ratios get even smaller as  $N_B$  increases. Thus, by narrowing down the search space to only those feasible SSVs, the search becomes much more efficient as the system scales up and the ‘‘curse of dimensionality’’ can be significantly alleviated.

### D. Case study

To evaluate the search efficiency within the original search space  $\mathcal{B}^{Ns}$  and the narrowed search space  $\mathcal{B}_f^{Ns}$ , a 10-cell RBS with design (d) in Fig. 1 is taken as an example. The RBS is discharged with a constant power of 70 W for 20 steps, and each step lasts 20 seconds. The initial SoCs for the 10 cells have a total SoC imbalance  $SoC_{ibl}^{tot} = 0.30$ , in which  $SoC_{ibl}^{tot}$  is defined as follows.

$$SoC_{ibl}^{tot} = \sum_{n=1}^{N_B} SoC_n - N_B \times \min_{n=1}^{N_B} SoC_n. \quad (32)$$

According to (32), when the system operation must be terminated because the minimum cell SoC has reached its lower limit for all cells,  $SoC_{ibl}^{tot}$  represents the total cell SoCs that remain unused.

Then, an RBS optimal control problem is formulated for minimizing the total SoC imbalance  $SoC_{ibl}^{tot}$  at the end of the last step. To solve this problem, the Genetic Algorithm

**Algorithm 1** Algorithm of parallel-then-series Configuration Enumeration

```

1: Define five cell position flags: the  $M_p$  at the beginning of a  $C_{ps}$  ( $FP$ ), the  $M_p$  at the middle of a  $C_{ps}$  ( $MP$ ), the  $M_p$  at the end of a  $C_{ps}$  ( $LP$ ), a  $M_s$  ( $S$ ), and bypassing ( $B$ ). Represent a  $C_{ps}$  by a vector consisting of all cell flags.
2: Initialize  $D$  as a  $N_B \times N_B \times 3$  list of cell flag vectors, and let  $D[i][j][:]$  represent the flag vectors with a total of  $i$  cells and meeting a terminal voltage level  $j$ .
3: If the last non-bypassed cell's position flag in a flag vector is  $FP$ ,  $S$ ,  $MP$ , or  $LP$ , place the flag vector into the sub-list  $D[i][j][0]$ ,  $D[i][j][1]$ ,  $D[i][j][1]$ , or  $D[i][j][2]$ , respectively.
4: Initialize  $D[1][1][0] \leftarrow [[FP]]$ 
5: Initialize  $D[1][1][1] \leftarrow [[S]]$ 
6: Initialize  $D[1][1][2] \leftarrow []$ 
7: for  $i \leftarrow 2$  to  $N_B$  do
8:   for  $j \leftarrow 1$  to  $i$  do
9:     if  $j = 1$  then
10:      Initialize  $all\_bypass \leftarrow [B] \times (i - 1)$ 
11:       $D[i][j][0].append(all\_bypass.append(FP))$ 
12:       $D[i][j][1].append(all\_bypass.append(S))$ 
13:    end if
14:     $D[i][j][0].extend([h.append(B) \mid h \in D[i - 1][j][0]])$ 
15:     $D[i][j][0].extend([h.append(FP) \mid h \in D[i - 1][j][0]])$ 
16:     $D[i][j][1].extend([h.append(B) \mid h \in D[i - 1][j][1]])$ 
17:     $D[i][j][1].extend([h.append(S) \mid h \in D[i - 1][j - 1][0] \text{ if } h.count(FP) > 1])$ 
18:     $D[i][j][1].extend([h.append(S) \mid h \in D[i - 1][j - 1][1]])$ 
19:    for  $n\_mp \leftarrow 2$  to  $i - 1$  do
20:       $D[i][j][1].extend([h.append(MP) \times n\_mp \mid h \in D[i - n\_mp][j - 1][0] \text{ if } h.count(FP) > 1])$ 
21:       $D[i][j][1].extend([h.append(MP) \times n\_mp \mid h \in D[i - n\_mp][j - 1][1]])$ 
22:    end for
23:     $D[i][j][2].extend([h.append(B) \mid h \in D[i - 1][j][2]])$ 
24:     $D[i][j][2].extend([h.append(LP) \mid h \in D[i - 1][j - 1][0] \text{ if } h.count(FP) > 1])$ 
25:     $D[i][j][2].extend([h.append(LP) \mid h \in D[i - 1][j - 1][1]])$ 
26:     $D[i][j][2].extend([h.append(LP) \mid h \in D[i - 1][j][2]])$ 
27:  end for
28: end for
29: return  $D[N_B][L_{vt}^{min} : L_{vt}^{max}][:]$ 

```

TABLE IV  
COMPARISON OF THE NUMBER OF FEASIBLE SSVs  $N_f(N_B, L_{vt})$  FOR RBSS WITH VARIOUS CELL NUMBERS AND TERMINAL VOLTAGE LEVELS.

$N_f(N_B, L_{vt})$	$N_B = 2$	$N_B = 3$	$N_B = 4$	$N_B = 5$	$N_B = 6$	$N_B = 7$	$N_B = 8$	$N_B = 9$	$N_B = 10$
$L_{vt} = 1$	3	7	15	31	63	127	255	511	1023
$L_{vt} = 2$	1	5	18	54	144	356	839	1919	4307
$L_{vt} = 3$	-	1	7	30	103	310	853	2200	5410
$L_{vt} = 4$	-	-	1	9	47	187	631	1907	5327
$L_{vt} = 5$	-	-	-	1	11	68	312	1186	3959
$L_{vt} = 6$	-	-	-	-	1	13	93	485	2063
$L_{vt} = 7$	-	-	-	-	-	1	15	122	714
$L_{vt} = 8$	-	-	-	-	-	-	1	17	155
$L_{vt} = 9$	-	-	-	-	-	-	-	1	19
$L_{vt} = 10$	-	-	-	-	-	-	-	-	1
No. of feasible SSVs = $\sum_{L_{vt}=1}^{N_B} N_f(N_B, L_{vt})$	4	13	41	125	369	1062	2999	8348	22978
No. of possible SSVs = $2^{5N_B-3}$	128	$4.096 \times 10^3$	$1.311 \times 10^5$	$4.194 \times 10^6$	$1.342 \times 10^8$	$4.295 \times 10^9$	$1.374 \times 10^{11}$	$4.398 \times 10^{12}$	$1.407 \times 10^{14}$
$\sum_{L_{vt}=1}^{N_B} N_f(N_B, L_{vt}) / 2^{5N_B-3}$	$3.125 \times 10^{-2}$	$3.174 \times 10^{-3}$	$3.128 \times 10^{-4}$	$2.980 \times 10^{-5}$	$2.749 \times 10^{-6}$	$2.473 \times 10^{-7}$	$2.182 \times 10^{-8}$	$1.898 \times 10^{-9}$	$1.633 \times 10^{-10}$

(GA) [23] is deployed, in which the population size, crossover probability, and mutation probability are set to 100, 0.8, and 0.1, respectively. The narrowed search space is examined in comparison with the complete search space composed of all possible SSVs. The evolutions of  $SoC_{ibl}^{tot}$  over generations using these two types of search space are compared in Fig. 9.

It can be seen from Fig. 9 that the obtained total SoC imbalance  $SoC_{ibl}^{tot}$  using the narrowed search space converges quickly to 0.031 after 220 generations. However, within

the same number of generations of search in the complete search space, the  $SoC_{ibl}^{tot}$  remains unchanged. Since there exist massive infeasible SSVs in the complete space, leading to short circuits, open circuits, and unacceptable system terminal voltage levels, it becomes difficult to select feasible actions consecutively in the GA, forcing the search to end prematurely. This case study shows the proposed algorithm for narrowing the search space to only feasible solution set can facilitate the fast convergence to the optimal solution.

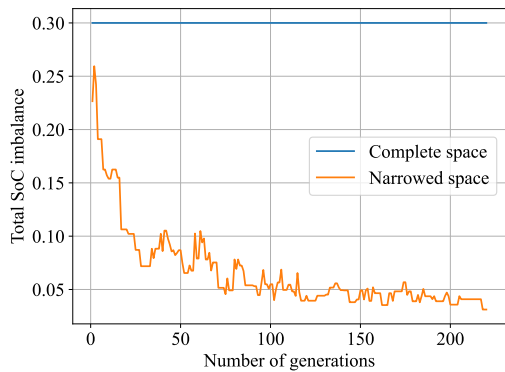


Fig. 9. Comparison of optimization results based on the complete search space and the narrowed search space.

## V. CONCLUSIONS

This study aims to address two fundamental challenges in the optimal control of RBSs: constructing the system plant expression during problem formulation and enhancing search efficiency during problem-solving.

The proposed unified modeling framework eliminates the need to frequently reconstruct the system plant during dynamic battery reconfiguration. This enables the formulation of optimal control problems for RBSs while significantly reducing computational time and storage requirements. Compared to experimental test results, the proposed RBS model demonstrates high accuracy in simulating dynamic current and voltage distributions within the system.

Furthermore, when solving the formulated RBS optimal control problems, an algorithm is proposed to narrow the complete search space to only feasible solutions, thereby not only dramatically enhancing search efficiency but also filtering out all configurations that could result in battery faults or unacceptable terminal voltages.

Building on these essential techniques for RBSs, a variety of optimal control problems can be formulated and efficiently solved to enhance system performance from multiple perspectives, including improving fault tolerance, optimizing energy storage and delivery, enhancing charge balance, and extending the remaining useful life.

## REFERENCES

- [1] Y. Wang, Q. Chao, L. Zhao, and R. Chang, "Assessment of wind and photovoltaic power potential in China," *Carbon Neutrality*, vol. 1, no. 1, p. 15, May 2022.
- [2] X. Zhang, L. Feng, X. Li, Y. Xu, L. Wang, and H. Chen, "Economic evaluation of energy storage integrated with wind power," *Carbon Neutrality*, vol. 2, no. 1, p. 16, Jul. 2023.
- [3] L. Lu, X. Han, J. Li, J. Hua, and M. Ouyang, "A review on the key issues for lithium-ion battery management in electric vehicles," *Journal of power sources*, vol. 226, pp. 272–288, 2013.
- [4] A. Barré, B. Deguilhem, S. Grolleau, M. Gérard, F. Suard, and D. Riu, "A review on lithium-ion battery ageing mechanisms and estimations for automotive applications," *Journal of Power Sources*, vol. 241, pp. 680–689, Nov. 2013.
- [5] X. Feng, M. Ouyang, X. Liu, L. Lu, Y. Xia, and X. He, "Thermal runaway mechanism of lithium ion battery for electric vehicles: A review," *Energy Storage Materials*, vol. 10, pp. 246–267, Jan. 2018.
- [6] S. Ci, N. Lin, and D. Wu, "Reconfigurable Battery Techniques and Systems: A Survey," *IEEE Access*, vol. 4, pp. 1175–1189, 2016.

- [7] T. Kim, W. Qiao, and L. Qu, "Series-connected self-reconfigurable multicell battery," in *2011 Twenty-Sixth Annual IEEE Applied Power Electronics Conference and Exposition (APEC)*. IEEE, 2011, pp. 1382–1387.
- [8] Y. Kim, S. Park, Y. Wang, Q. Xie, N. Chang, M. Poncino, and M. Pedram, "Balanced reconfiguration of storage banks in a hybrid electrical energy storage system," in *2011 IEEE/ACM International Conference on Computer-Aided Design (ICCAD)*. IEEE, 2011, pp. 624–631.
- [9] S. Steinhorst, Z. Shao, S. Chakraborty, M. Kauer, S. Li, M. Lukasiewicz, S. Narayanaswamy, M. U. Rafique, and Q. Wang, "Distributed reconfigurable battery system management architectures," in *2016 21st Asia and South Pacific Design Automation Conference (ASP-DAC)*. IEEE, 2016, pp. 429–434.
- [10] H. Visairo and P. Kumar, "A reconfigurable battery pack for improving power conversion efficiency in portable devices," in *2008 7th International Caribbean Conference on Devices, Circuits and Systems*. IEEE, 2008, pp. 1–6.
- [11] M. Alahmad, H. Hess, M. Mojarradi, W. West, and J. Whitacre, "Battery switch array system with application for JPL's rechargeable micro-scale batteries," *Journal of Power Sources*, vol. 177, no. 2, pp. 566–578, 2008.
- [12] S. Ci, J. Zhang, H. Sharif, and M. Alahmad, "Dynamic reconfigurable multi-cell battery: A novel approach to improve battery performance," in *2012 Twenty-Seventh Annual IEEE Applied Power Electronics Conference and Exposition (APEC)*. IEEE, 2012, pp. 439–442.
- [13] M. Alahmad, H. Hess, M. Mojarradi, W. West, and J. Whitacre, "Battery switch array system with application for JPL's rechargeable micro-scale batteries," *Journal of Power Sources*, vol. 177, no. 2, pp. 566–578, 2008.
- [14] Z. Zhang, Y.-Y. Cai, Y. Zhang, D.-J. Gu, and Y.-F. Liu, "A distributed architecture based on microbank modules with self-reconfiguration control to improve the energy efficiency in the battery energy storage system," *IEEE Transactions on Power Electronics*, vol. 31, no. 1, pp. 304–317, 2015.
- [15] W. Han, C. Zou, L. Zhang, Q. Ouyang, and T. Wik, "Near-fastest battery balancing by cell/module reconfiguration," *IEEE Transactions on Smart Grid*, vol. 10, no. 6, pp. 6954–6964, 2019.
- [16] F. Altaf, B. Egardt, and L. Johannesson Mårdh, "Load Management of Modular Battery Using Model Predictive Control: Thermal and State-of-Charge Balancing," *IEEE Transactions on Control Systems Technology*, vol. 25, no. 1, pp. 47–62, Jan. 2017.
- [17] Taesic Kim, Wei Qiao, and Liyan Qu, "Power Electronics-Enabled Self-X Multicell Batteries: A Design Toward Smart Batteries," *IEEE Transactions on Power Electronics*, vol. 27, no. 11, pp. 4723–4733, Nov. 2012.
- [18] A. Badam, R. Chandra, J. Dutra, A. Ferrese, S. Hodges, P. Hu, J. Meinershagen, T. Moscibroda, B. Priyantha, and E. Skiani, "Software defined batteries," in *Proceedings of the 25th Symposium on Operating Systems Principles*. Monterey California: ACM, Oct. 2015, pp. 215–229.
- [19] W. Han, T. Wik, A. Kersten, G. Dong, and C. Zou, "Next-Generation Battery Management Systems: Dynamic Reconfiguration," *IEEE Industrial Electronics Magazine*, vol. 14, no. 4, pp. 20–31, Dec. 2020.
- [20] S. C. Hageman, "Simple PSpice models let you simulate common battery types," *EDN*, vol. 38, no. 22, p. 117, 1993.
- [21] "N-Channel 25 V (D-S) MOSFET," *Vishay Siliconix*, 2016.
- [22] BH. SHH and GAT. EE, "PNGV battery test manual," 1999.
- [23] J. H. Holland, *Adaptation in Natural and Artificial Systems: An Introductory Analysis with Applications to Biology, Control, and Artificial Intelligence*. MIT press, 1992.